

Efficient hydrophilicity improvement of titanium surface by plasma jet in micro-hollow cathode discharge geometry

Peng-Ying Jia(贾鹏英), Han-Xiao Jia(贾焓潇), Jun-Xia Ran(冉俊霞), Kai-Yue Wu(吴凯玥), Jia-Cun Wu(武珈存), Xue-Xia Pang(庞学霞), and Xue-Chen Li(李雪辰)

Citation: Chin. Phys. B, 2023, 32 (**8**): 085202. DOI: 10.1088/1674-1056/acbde9

Journal homepage: http://cpb.iphy.ac.cn; http://iopscience.iop.org/cpb

What follows is a list of articles you may be interested in

Influence of oxygen addition on the discharge characteristics of an argon plasma jet at atmospheric pressure

Junyu Chen(陈俊宇), Na Zhao(赵娜), Jiacun Wu(武珈存), Kaiyue Wu(吴凯玥), Furong Zhang(张芙蓉),Junxia Ran(冉俊霞), Pengying Jia(贾鹏英), Xuexia Pang(庞学霞), and Xuechen Li(李雪辰)

Chin. Phys. B, 2022, 31 (**6**): 065205. DOI: 10.1088/1674-1056/ac601a

Sterilization of mycete attached on the unearthed silk fabrics by an atmospheric pressure plasma jet

Rui Zhang(张锐), Jin-song Yu(於劲松), Jun Huang(黄骏), Guang-liang Chen(陈光良), Xin Liu(刘欣), Wei Chen(陈维), Xing-quan Wang(王兴权), Chao-rong Li(李超荣)

Chin. Phys. B, 2018, 27 (**5**): 055207. DOI: 10.1088/1674-1056/27/5/055207

Characteristic plume morphologies of atmospheric Ar and He plasma jets excited by a pulsed microwave hairpin resonator

Zhao-Quan Chen(陈兆权), Ben-Kuan Zhou(周本宽), Huang Zhang(张煌), Ling-Li Hong(洪伶俐), Chang-Lin Zou(邹长林), Ping Li(李平), Wei-Dong Zhao(赵卫东), Xiao-Dong Liu(刘晓东), Olga Stepanova, A A Kudryavtsev

Chin. Phys. B, 2018, 27 (**5**): 055202. DOI: 10.1088/1674-1056/27/5/055202

Characteristics of helium DC plasma jets at atmospheric pressure with multiple cathodes

Cheng Wang(王城), Zelong Zhang(张泽龙), Haichao Cui(崔海超), Weiluo Xia(夏维珞), Weidong Xia(夏维东)

Chin. Phys. B, 2017, 26 (**8**): 085207. DOI: 10.1088/1674-1056/26/8/085207

LIF diagnostics of hydroxyl radical in a methanol containing atmospheric-pressure plasma jet

Mu-Yang Qian(钱沐杨), San-Qiu Liu(刘三秋), Xue-Kai Pei(裴学凯), Xin-Pei Lu(卢新培), Jia-Liang Zhang(张家良), De-Zhen Wang(王德真)

Chin. Phys. B, 2016, 25 (**10**): 105205. DOI: 10.1088/1674-1056/25/10/105205

Efficient hydrophilicity improvement of titanium surface by plasma jet in micro-hollow cathode discharge geometry

Peng-Ying Jia(贾鹏英)[1], Han-Xiao Jia(贾焓潇)[1], Jun-Xia Ran(冉俊霞)[1], Kai-Yue Wu(吴凯玥)[2], Jia-Cun Wu(武珈存)[2], Xue-Xia Pang(庞学霞)[1], and Xue-Chen Li(李雪辰)[1,2,†]

[1] *College of Physics Science & Technology, Hebei University, Baoding* 071002, *China*
[2] *Institute of Life Science & Green Development, Hebei University, Baoding* 071002, *China*

(Received 2 December 2022; revised manuscript received 15 February 2023; accepted manuscript online 22 February 2023)

Surface hydrophilicity improvement of titanium (Ti) is of great significance for the applications of the important biomaterial. In this study, efficient hydrophilicity on the Ti surface is improved by an air plasma jet generated by a micro-hollow cathode discharge (MHCD) geometry. Elementary discharge aspects of the plasma jet and surface characteristics of the Ti surface are investigated by varying dissipated power (P_d). The results show that the plasma jet can operate in a pulsed mode or a continuous mode, depending on P_d. The plume length increases with P_d and air flow rate increasing. By optical emission spectroscopy, plasma parameters as a function of P_d are investigated. After plasma treatment, water contact angel (WCA) of the Ti sample decreases to a minimum value of 15° with P_d increasing. In addition, the surface topography, roughness, and content of chemical composition are investigated by scanning electron microscopy (SEM), atomic force microscopy (AFM), and x-ray photoelectron spectroscopy (XPS) with P_d increasing. The results show that Ti–O bond and O–H group on the Ti surface are beneficial to the improvement of the hydrophilicity of Ti surface.

Keywords: plasma jet, plasma treatment, plasma parameters, discharge aspects

PACS: 52.80.Tn, 52.77.Bn, 52.70.Kz ,52.50.Dg **DOI:** 10.1088/1674-1056/acbde9

1. Introduction

Ti and its alloys are frequently applied in dental implants,[1,2] orthopedic applications,[3] and aerospace industries[4,5] due to their integrating excellent mechanical strength,[6,7] corrosion resistance,[8] and biocompatibility.[6,9] However, the hydrophilicity of Ti surface is not satisfactory, leading to poor bonding interface strength,[5,10] which makes titanium workpieces hard to join together. To make the interconnection between titanium workpieces reliable, stable and strong, the bonding interface strength of Ti needs to be enhanced. The improvement of hydrophilicity can enhance the interface bonding strength, which is a hot issue in the applications of Ti and its alloys.[10–17]

Various methods have been used to improve the surface hydrophilicity of Ti and its alloys, including micro/nanotopographical modification, sandblasting, acid etching, anodic oxidizing, and a combination of these methods.[18–20] Unlike these ordinary methods, low-temperature plasma has provided a green modification approach, which has the advantages of low energy consumption, safety, and no pollution.[21–24] However, the hydrophilicity of the Ti sample was not improved remarkably after 2-min treatment with dielectric barrier discharge (DBD).[25] With a sufficiently long exposure (15 min),[26] the water contact angel (WCA) of the Ti surface decreased from 89.6° to 45.4°.[27]

In contrast to plasma confined between the DBD electrodes, plasma jet could generate a plasma plume in the open air,[28–33] which is more desirable, especially in the surface modification of three-dimensional (3D) workpiece. Although plasma jet had various configuration,[34] DBD was popular to be used in this area. Compared with the DBD jet, micro-hollow cathode discharge (MHCD) jet could produce a plasma plume with a higher electron density.[35,36] Hence, efficient surface modification of Ti was expected with the MHCD jet. Up to now, Ti surface modification have been implemented with the MHCD jet excited by an alternating-current voltage.[37–40] Under such an excitation, the duty ratio is very low due to the intermittently pulsed discharge. To further improve the efficiency of plasma modification, the duty ratio of the MHCD jet should be increased.

In this paper, an MHCD plasma jet with a continuous mode (duty ratio is 100%) is produced and efficient treatment of the Ti surface is realized. In addition to discharge characteristics, WCA, surface morphology, and chemical compositions of the Ti surface are evaluated after being treated by the plasma jet with different values of P_d.

2. Experimental setup

Figure 1 shows a schematic diagram of the experimental setup. A tungsten needle with a radius of 0.5 mm and a tip radius of about 250 μm was coaxially wrapped by a quartz tube with inner diameter of 3.0 mm and outer diameter of 5.0 mm. The needle anode was connected via a shunt resistor ($R = 1.0$ MΩ) to the high-voltage output of a power supply

†Corresponding author. E-mail: plasmalab@126.com; xuechenli@126.com
© 2023 Chinese Physical Society and IOP Publishing Ltd

(Glassman KR20R150). A 10.0-cm-long tube was placed vertically, whose bottom was attached to a molybdenum disk with a diameter of 15.0 mm and a thickness of 1.0 mm, leaving a 2.0-mm gap between the disk and the needle. A hole with a diameter of 0.8 mm was drilled in the center of the disk (the cathode). Hollow cathode discharge (HCD) was generated between an anode with an arbitrary shape and a cathode that contains a hollow structure.[41] At atmospheric pressure, the discharge existed in the form of a cathode hole with a diameter of hundreds of microns,[42] which indicates the corresponding MHCD. As reported by Moshkunov *et al.*[43] plasma jet in the MHCD geometry could operate in flowing air. The cathode hole of our plasma jet had a diameter of 0.8 mm. Hence, it belonged to MHCD plasma jet, which is fed with air via a flow meter (Sevenstar CS200A). For the feeding air, its default temperature, humidity, and pressure were 22 °C, 21%, and 1.01×10^5 Pa, respectively. The applied voltage was detected by a probe (Tektronix P6015A), and the discharge current was measured by a coil (Pearson 8600). Their waveforms were monitored by a digital oscilloscope (Tektronix DPO4104). A plasma plume emanated from the jet orifice, whose image (Fig. 1) was captured by a single lens reflex camera (Canon EOS 7D). Optical emission spectrum was collected by a spectrometer (PI ACTON SP2750) with a grating of 2400 mm^{-1}.

Before being treated by plasma, commercial pure titanium rectangles (grade II) with 7.0 mm×10.0 mm area and 1.0-mm thickness were polished with 2000 mesh silicon carbide paper, and then ultrasonically cleaned for 15-min successively by using acetone, ethanol, and distilled water. Finally, the samples were dried in room-temperature air. During plasma treatment, the samples that just touch the plume tail were held horizontally by a jig on an x–y stage. The samples were scanned along gridlines similar to those reported in Ref. [40]. The sample scan velocity determined the treatment time of the sample due to the constant sample size. The static WCA was measured with a contact angle analyzer (Powereach JC2000D4) through dropping 2.0-μL deionized water on the samples.[24] An average WCA value was obtained after five measurements. Moreover, the samples were analyzed by using x-ray photoelectron spectroscopy (XPS) (Thermo Fisher ESCALAB250Xi) with a base pressure of about 2×10^{-9} Pa. X-rays have a spot area of over a 500-μm diameter, which comes from a monochromatic Al K$\alpha_{1,2}$ radiation at 1486.6 eV.[24] All spectra were corrected with the main C 1s peak of carbon atoms (284.8 eV) as an internal reference. An atom force microscopy (AFM) (OXFORD MFP-3D Origin) was used to evaluate surface morphology, which operated in an alternating current (AC) air topography mode with a scan rate of 1.0 Hz and a driving frequency of 139.922 kHz. In addition, a scanning electron microscope (SEM) (FEI, Nova NanoSEM450) was applied to the samples to study their morphological changes.

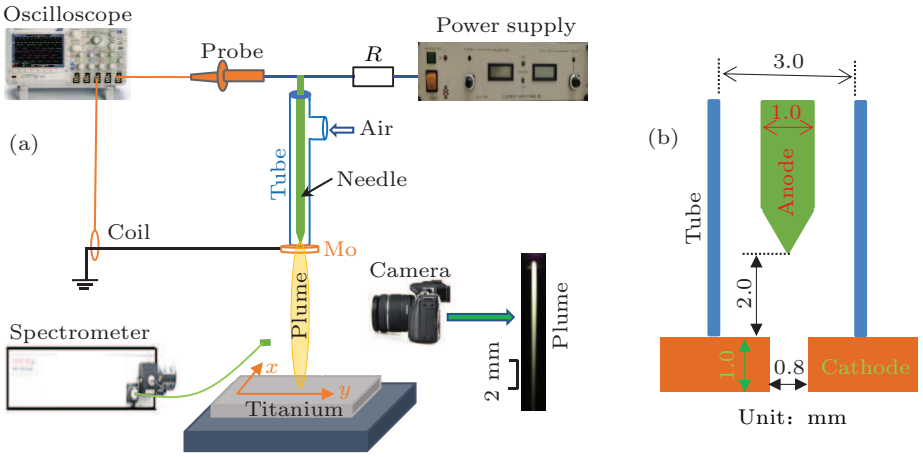


Fig. 1. (a) Schematic diagram of experimental setup. The plume image is obtained at t_{exp}, Q, and P_d of 0.1 s, 1.5 L/min, and 16.0 W, respectively. (b) Sectional view of MHCD plasma jet.

3. Results and discussion

Figure 2 illustrates waveforms of applied voltage and discharge current under different values of P_d, which are calculated from the voltage waveform and current waveform.[44] For lower P_d, both applied voltage and discharge current vary with time. Applied voltage keeps increasing with time elapsing until it reaches the voltage threshold for breakdown, leading the impedance of the circuit to decrease suddenly. Resultantly, the applied voltage decreases sharply and discharge current increases abruptly. However, the discharge quenches after a while. Then, the applied voltage recovers with time going on and evokes the next discharge, which is similar to that reported in a plasma brush.[23,28] The waveforms of the voltage and the current are in the form of pulses, so this existing mode is defined as the pulsed mode. Unlike the pulsed mode, the applied voltage and the discharge current are invariant with time under higher P_d, which is named a continuous mode.[45,46]

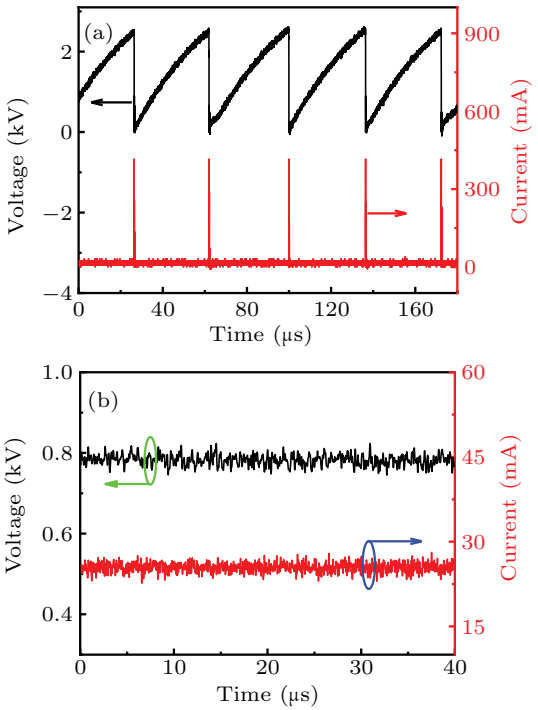


Fig. 2. Waveforms of applied voltage and discharge current with $P_d = 4.0$ W (a) and 20.0 W (b), and $Q = 1.5$ L/min.

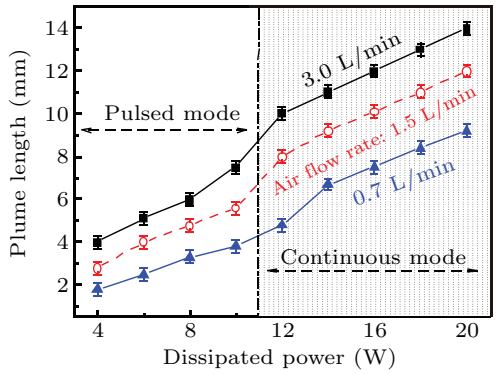


Fig. 3. Variations of length of plasma plume with P_d.

Plasma plume length as a function of P_d is investigated, and the results are shown in Fig. 3. One can see that in the two discharge modes, the plume length increases with P_d increasing. Moreover, air flow rate can influence the length of the plume, specifically, when the flow rate rises in the range below 3.0 L/min, the plume becomes longer. The dependence of plume length on P_d and air flow rate can be explained as follows. For the gas-flow driven plasma jet,[47] plasma is first generated between the two electrodes. After being blown out, a plume is formed in the downstream region. During moving outside the plasma jet, the plasma degenerates because of the recombination between electrons and ions. Owing to the moving velocity increasing, the degenerate plasma will travel a longer distance with air flow rate increasing. As a result, the plume becomes longer with flow rate rising. Moreover, electron density increases with P_d increasing, which will be mentioned later. The higher density plasma will experience a longer degeneration time, leading the plume length to increase with P_d increasing.

Figure 4(a) shows an optical emission spectrum scanned from 300 nm to 800 nm for the two discharge modes. It can be found that various radicals and reactive species are produced in the plasma plume, whose emission intensities are higher in the continuous mode than those in the pulsed mode. The spectra mainly include the second positive system of N_2 ($C^3\Pi_u \rightarrow B^3\Pi_g$),[29–31,48,49] where the dominant emission band heads at 337.1 nm, the first positive system of N_2 ($B^3\prod_g \rightarrow A^3\sum_u^+$),[50–52] the first negative system of N_2^+ ($B^2\sum_g^+ - X^2\sum_g^+$),[32,53,54] and OH transition ($A^2\Sigma^+ \rightarrow X^2\Pi$).[33,55,56] Furthermore, the spectral line of O I ($3p^5P \rightarrow 3s^5S$) can also be discerned at 777.4 nm.[44] Hence, one can deduce that the active species in the plasma include electrons, positive ions (N_2^+), excited nitrogen molecules (N_2 ($C^3\Pi_u$)) and N_2 ($B^3\Pi_g$)), atomic oxygen, and OH radical. Hence, the spectral line intensities of the active species are investigated as a function of P_d. It can be seen from Fig. 4(b) that the spectral line intensities increase with P_d increasing. In the plasma plume, electrons collide with neutral particles to produce active species. Hence, the high electron density is conducive to the generation of active species. As a result, the increase of line intensities indicates that electron density increases with P_d increasing.

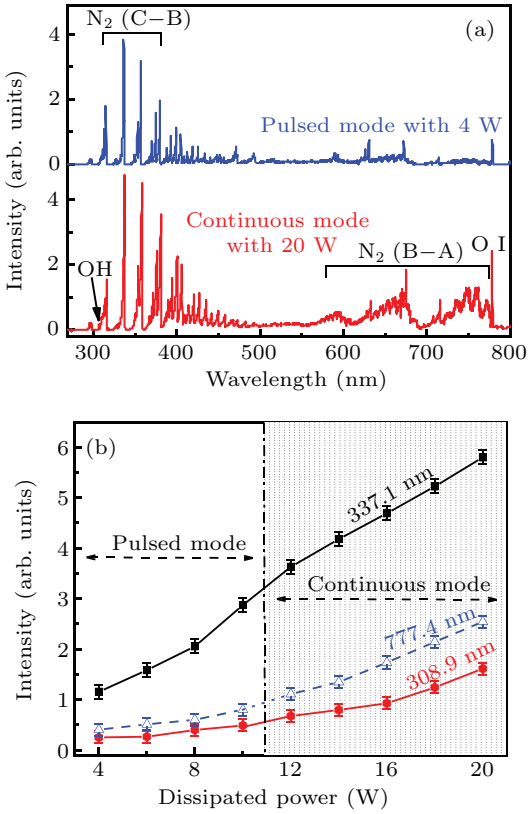


Fig. 4. (a) The 300 nm–800 nm scanned optical emission spectrum from plasma plume. (b) Variations of spectral line intensity with P_d.

In addition, plasma parameters such as electron temperature and electron density can be reflected from the inten-

sity ratio of spectral lines.[57–61] Here, the intensity ratio in the range from 391.4 nm to 337.1 nm is used to reflect electron temperature,[32,57,58] and the intensity ratio ranging from 371.1 nm to 380.4 nm is sensitive to electron density.[62,63] Hence, the intensity ratios of these lines are investigated as a function of P_d, and the results are shown in Fig. 5(a). It can be deduced that both electron temperature and electron density increase with P_d increasing. In addition, the vibrational temperature can be calculated from the second positive system of N_2 ($C^3\Pi_u \rightarrow B^3\Pi_g$), and gas temperature can be estimated from OH ($A^2\Sigma^+ \rightarrow X^2\Pi$).[64,65] As shown in Fig. 5(b), both vibrational temperature and gas temperature of the plasma plume increase with P_d increasing.

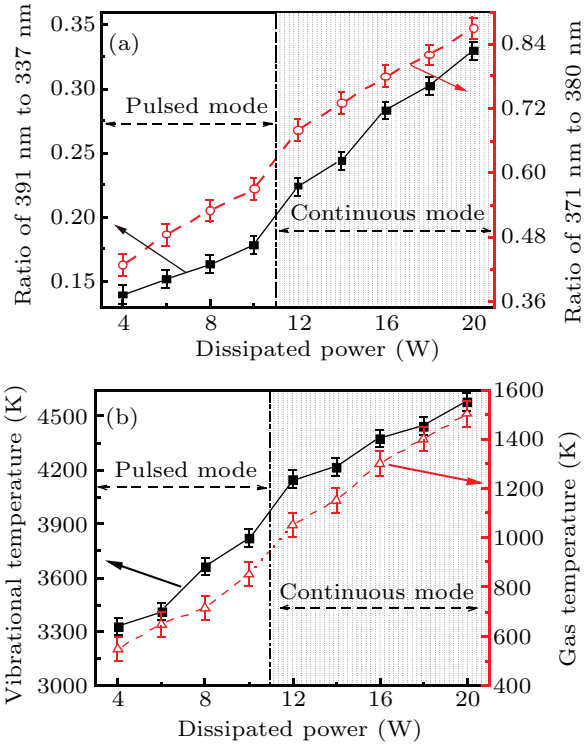


Fig. 5. Variations of (a) line intensity ratios with dissipated power and (b) variations of vibration temperature and gas temperature with dissipated power at $Q = 1.5$ L/min.

Figure 6(a) shows the variations of WCA with dissipated power of a single-scanned sample for pulsed mode and continuous mode. It is obvious that WCA of the treated sample decreases with P_d increasing, implying that the hydrophilicity is improved with P_d increasing. Under a constant P_d, the hydrophilicity is better with a lower scan velocity (v_s). Moreover, trace water vapor is introduced into the air flow, resulting in 49% air humidity (H). Under constant v_s and P_d, WCA decreases with H increasing. With P_d increasing and v_s decreasing, a minimum value of WCA of about 15° is reached. Furthermore, it can be seen from Fig. 6(b) that in the first five days WCA increases steeply, then increases slowly, and finally reaches a constant value. WCA after aging becomes lower for the samples treated with higher P_d.

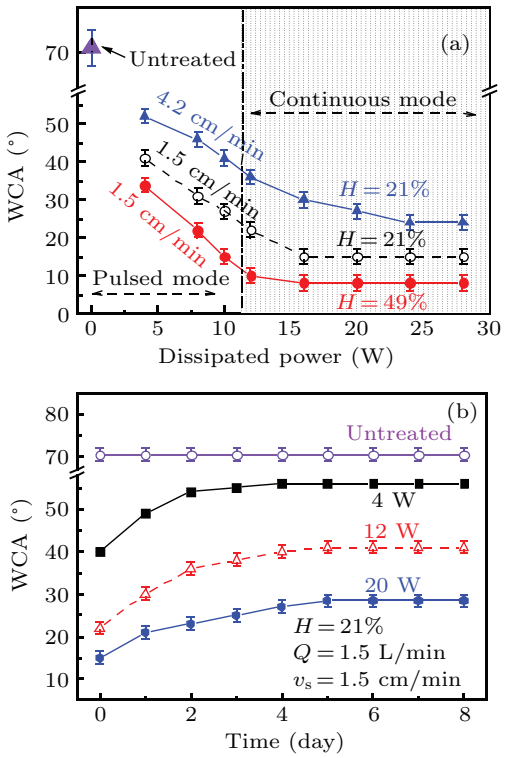


Fig. 6. (a) Variations of WCA with P_d of the single-scanned sample, and (b) variations of WCA with time, showing aging behaviors of single-scan sample with different values of P_d.

The SEM images (Fig. 7) show the difference in topography between the samples untreated and treated with different values of P_d. The untreated surface exhibits some pronounced machining marks. For the plasma treated sample (4.0 W), some irregular topographies appear, which come from the production of oxygen-containing polar group, such as Ti–O, which will be discussed later. With P_d increasing to 12.0 W, the area of irregular topographies increases. With a P_d of 20.0 W, the surface of titanium is covered with more oxygen-containing polar groups.

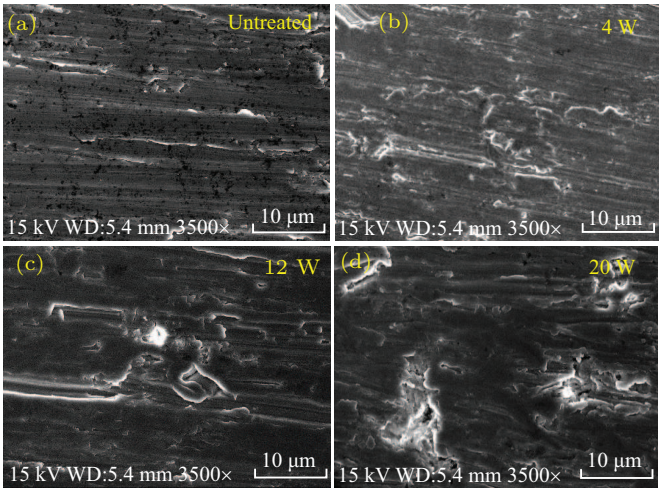


Fig. 7. SEM images at 3500× magnification of (a) untreated surface and treated surface with single scanning under v_s of 1.5 cm/min, Q of 1.5 L/min, and H of 21% at $P_d = 4.0$ W (b), 12.0 W (c), and 20.0 W (d).

The AFM images of the Ti samples are also recorded after plasma treatment, and the results are presented in Fig. 8. Then, the values of average roughness (R_a) and the root-mean-square (RMS) roughness (R_q) of the Ti surface can be obtained as listed in Table 1, in which each value is averaged through five measurements. Owing to machining marks, R_a of the untreated surface is 68.3±2.5 nm. Some small peaks appear on the surface treated with 4.0 W, and R_a reaches 78.4±2.5 nm. Besides these small peaks, some higher peaks appear on the surface treated with 12.0 W. Under such conditions, R_a reaches 79.8±2.5 nm. After plasma treatment with 20.0 W, the peaks turn higher and R_a reaches 82.5±2.5 nm. Owing to the surface chemical element cleaning and reconstruction caused by plasma treatment, the morphology and the roughness are changed. The increase in R_a is beneficial to the hydrophilicity improvement.[39]

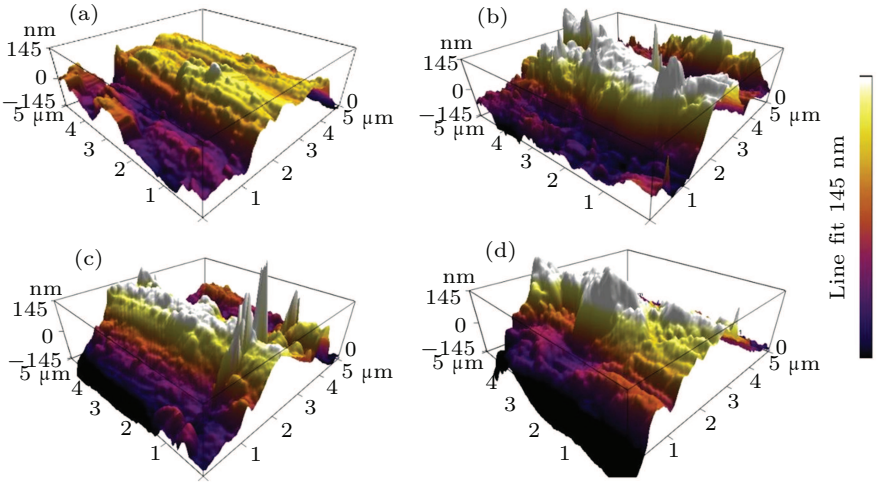


Fig. 8. AFM images of the surface, with panels (a)–(d) corresponding to panels 7(a)–7(d), respectively.

Table 1. Values of average roughness (R_a) and root-mean-square (RMS) roughness (R_q) at different values of P_d.

Power	Untreated	4 W	12 W	20 W
R_a (nm)	68.3±2.5	78.4±2.5	79.8±2.5	82.5±2.5
R_q (nm)	80.2±3.0	94.0±3.0	94.2±3.0	96.5±3.0

During plasma treatment, active species impinge on the sample surface, breaking the chemical bonds (C–C, C–H, and C–O bonds) and inducing the chemical reactions.[66,67] Then, XPS is used to analyze the chemical compositions of the Ti specimen with and without plasma treatment. Figures 9(a)–9(d) show the survey XPS, high-resolution XPS of O 1s, Ti 2p, and C 1s for the sample treated with different values of P_d, respectively. One can see from Fig. 9(a) that the intensity and binding energy of C 1s decrease, while those of Ti 2p and O 1s increase with P_d increasing. As shown in Fig. 9(b), the intensity of Ti–O at binding energy of 530.0 eV increases with P_d increasing, implying that more Ti–O groups are produced with P_d increasing. In addition, the second peak located at 532.0 eV comes from O–H group [14,39], whose intensity increases with P_d and H increasing. The production of oxygen-containing polar groups (Ti–O and O–H) are beneficial to improving the surface hydrophilicity.[14] The better hydrophilicity of the sample treated with a higher H results from the generation of more O–H groups on the Ti surface. Figure 9(c) shows that the peak intensities of $Ti2p_{1/2}$ (464.2 eV) and $Ti2p_{3/2}$ (458.5 eV) increase with P_d increasing. Figure 9(d) shows the dominant peak corresponding to C–H at binding energy of 284.8 eV, whose intensity weakens with P_d increasing. Furthermore, the peak intensity corresponding to C–O at binding energy of 286.1 eV decreases with P_d increasing, which is consistent with previous result.[39]

Through Avantage software, the concentration of chemical compositions can be obtained from XPS as listed in Table 2. It can be seen that with the increase of P_d, the percentage of C 1s decreases from 47.93% to 24.84%, while the percentage of O 1s and Ti 2p increase from 36.90% to 49.24% and from 15.17% to 25.92%, respectively. The variations of the chemical compositions are analyzed as follows. The reduction of carbon is related to the cleaning effect of the organic substance left on the surface of the specimen due to plasma treatment.[1] The increase of oxygen can be attributed to surface modified by connecting a large number of oxygen-bonded functional groups (Ti–O and O–H) to the surface of substrate.[14] At the same time, the generation of more Ti–O (or TiO_2) groups arise from the increase of Ti 2p. In the analysis of O 1s (Table 3), the relative percentage of Ti–O groups increases from 42.80% to 62.42%, while the relative percentage of O–H groups decreases from 57.20% to 37.58% with the increase of P_d. The Ti–O group is produced during the reaction with atomic oxygen in the plasma, while O–H group on the sample surface is attributed to OH radical in the plasma. Both Ti–O and O–H groups are beneficial to the improvement of surface hydrophilicity.

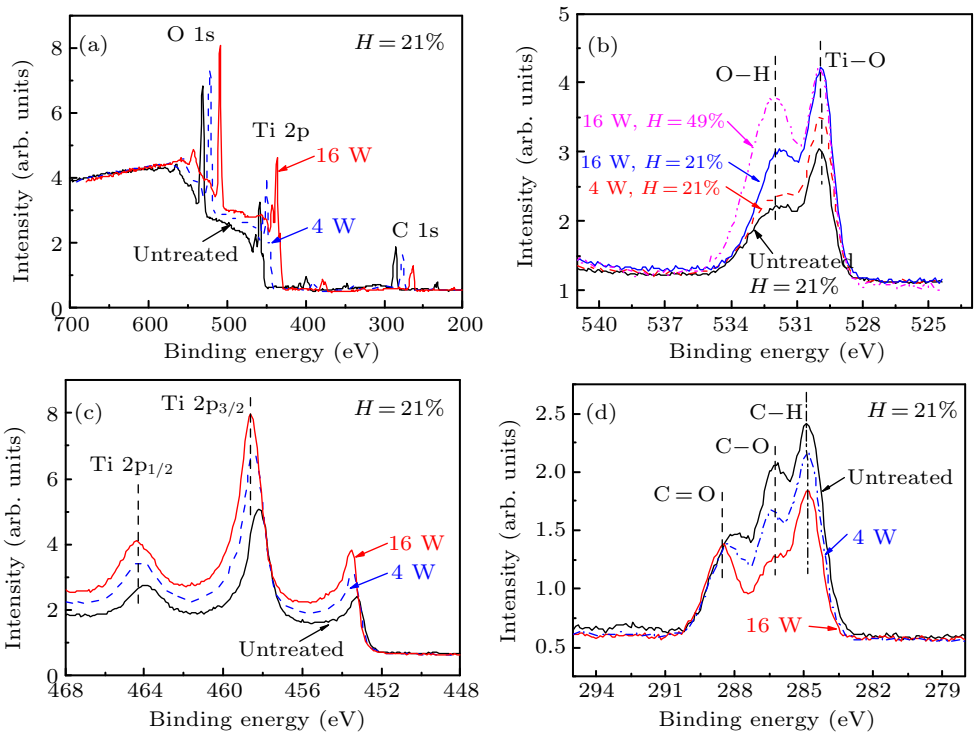


Fig. 9. (a) Survey XPS, (b) high-resolution XPS of O 1s, (c) Ti 2p, and (d) C 1s for untreated and single-scanned samples with different values of P_d, with other parameters being the same as those in Fig. 7.

Table 2. Percentages of chemical composition on untreated and treated titanium surface with single scanning at different values of P_d.

Power (W)	Atomic percent		
	C 1s (%)	Ti 2p (%)	O 1s (%)
Untreated	47.93	15.17	36.90
4	44.34	15.70	39.96
8	39.32	17.09	43.59
12	32.25	21.31	46.44
16	26.86	23.98	49.16
20	24.84	25.92	49.24

Table 3. Area percentages of O 1s peak components on untreated and treated titanium surface with single scanning at different values of P_d.

Power (W)	O 1s	
	Ti–O (%)	O–H (%)
Untreated	42.80	57.20
4	53.05	46.95
8	55.08	44.92
12	59.45	40.55
16	61.30	38.70
20	62.42	37.58

4. Conclusions

In summary, an air plasma jet in an MHCD configuration has been constructed to generate a plasma plume with a high electron density. The results show that the plasma jet operates in the pulsed mode with lower P_d and in the continuous mode with higher P_d. In addition to the discharge mode transition, the plume length increases with P_d or air flow rate increasing. It is found that the spectral intensity increases with P_d increasing, indicating more reactive species are produced in the plasma plume with P_d increasing. Moreover, plasma parameters including electron density, electron temperature, vibrational temperature, and gas temperature increase with P_d increasing. The Ti surface modification with a high efficiency is realized by using the dense electron plasma jet, which is revealed by scanning the sample. After a single scan, the WCA of the Ti surface decreases with P_d increasing to a minimal value of about 15°. Moreover, the surface hydrophilicity is better with lower v_s and higher H. After aging, better hydrophilicity is obtained at higher P_d. In addition, the increase of P_d can produce more oxygen-containing molecular groups, change the surface morphology, and increase the surface roughness. The XPS results reveal that oxygen-containing molecular group (Ti–O) is produced during plasma modification. Both the production of TiO_2 and the increase of roughness contribute to the hydrophilicity improvement of the Ti samples.

Acknowledgements

Project supported by the National Natural Science Foundation of China (Grant Nos. 51977057 and 11875121), the Natural Science Foundation of Hebei Province, China (Grant Nos. A2020201025 and A2022201036), the Natural Science Interdisciplinary Research Program of Hebei University, China (Grant Nos. DXK201908 and DXK202011), the Postgraduate's Innovation Fund Project of Hebei Province, China (Grant Nos. CXZZBS2019023 and CXZZBS2019029), and

the Post-graduate's Innovation Fund Project of Hebei University, China (Grant Nos. HBU2021ss063, HBU2021bs011, and HBU2022bs004).

References

[1] Jang K J, Kang J H, Sakthiabirami K, Lim H P, Yun K D, Yim E K, Oh G J, Yang H S, Lee K K and Park S W 2019 *J. Nanosci. Nanotechnol.* **19** 2154

[2] Ko Y M, Myung S W, Jung S C and Kim B H 2015 *J. Nanosci. Nanotechnol.* **15** 196

[3] Xing H Y, Li R Y, Wei Y J, Ying B D, Li D D and Qin Y G 2020 *Front. Bioeng. Biotechnol.* **8** 367

[4] Zhou B, Wang Y R, Zheng K, Ma Y, Wang Y S, Yu S W and Wu Y C 2020 *Chin. Phys. B* **29** 126101

[5] Akram M, Jansen K M B, Ernst L J and Bhowmik S 2011 *Int. J. Adhes. Adhes.* **31** 598

[6] Cáceres D, Munuera C, Ocal C, Jiménez J A, Gutiérrez A and López M FF 2008 *Acta Biomater.* **4** 1545

[7] Jang M H, Park Y B, Kwon J S, Kim Y J and Lee J H 2021 *Materials* **14** 1942

[8] Casagrande R B, Kunst S R, Beltrami L V R, Aguzzoli C, Brandalise R N and Malfatti C F 2018 *J. Coat. Technol. Res.* **15** 1089

[9] Oliveira W F, Arruda I R S, Silva G M M, Machado G, Coelho L C B B and Correia M T S 2017 *Mater. Sci. Eng. C* **81** 597

[10] Hirano M, Yamane M and Ohtsu N 2020 *Surf. Interface Anal.* **52** 835

[11] Gittens R A, Scheideler L, Rupp F, Hyzy S L, Geis-Gerstorfer J, Schwartz Z and Boyan B D 2014 *Acta Biomater.* **10** 2907

[12] Aita H, Hori N, Takeuchi M, Suzuki T, Yamada M, Anpo M and Ogawa T 2009 *Biomaterials* **30** 1015

[13] Le Guéhennec L, Soueidan A, Layrolle P and Amouriq Y 2007 *Dent. Mater.* **23** 844

[14] Wang L, Wang W W, Zhao H M, Liu Y S, Liu J and Bai N 2020 *ACS Omega* **5** 3996

[15] Lee M J, Kwon J S, Jiang H B, Choi E H, Park G and Kim K M 2019 *Sci. Rep.* **9** 1938

[16] Kwon J S, Choi S H, Choi E H, Kim K M and Chu P K 2020 *Int. J. Mol. Sci.* **21** 6085

[17] Buxadera-Palomero J, Fricke K, Reuter S, Gil F J, Rodriguez D and Canal C 2021 *Appl. Sci.* **11** 662

[18] Kim S H, Lee S J, Cho I S, Kim S K and Kim T W 2009 *Angle Orthod.* **79** 899

[19] Gittens R A, Olivares-Navarrete R, Cheng A, Anderson D M, McLachlan T, Stephan I, Geis-Gerstorfer J, Sandhage K H, Fedorov A G, Rupp F, Boyan B D, Tannenbaum R and Schwartz Z 2013 *Acta Biomater.* **9** 6268

[20] Choi S H, Jang S H, Cha J Y and Hwang C J 2016 *Am. J. Orthod.* **149** 31

[21] Zhang R, Yu J S, Huang J, Chen G L, Liu X, Chen W, Wang X Q and Li C R 2018 *Chin. Phys. B* **27** 055207

[22] Katahira K, Mifune N and Komotori J 2019 *CIRP Annals* **68** 201

[23] Li X C, Liu R J, Li X N, Gao K, Wu J C, Gong D D and Jia P Y 2019 *Phys. Plasmas* **26** 023510

[24] Wu J C, Wu K Y, Chen J Y, Song C H, Jia P Y and Li X C 2021 *Plasma Sci. Technol.* **23** 085504

[25] Lapitskaya V A, Kuznetsova T A, Rogachev A A, MeI'nikova G.B, Chizhik S A and Kotov D A 2019 *J. Eng. Phys. Thermophys.* **92** 1349

[26] Attri P, Sarinont T, Kim M, Amano T, Koga K, Cho A E, Choi E H and Shiratani M 2015 *Sci. Rep.* **5** 17781

[27] Choi S H, Jeong W S, Cha J Y, Lee J H, Lee J H, Lee K J, Yu H S, Choi E H, Kim K M and Hwang C J 2017 *Dent. Mater.* **33** 1426

[28] Li X C, Wu J C, Jia B Y, Wu K Y, Kang P C, Zhang F R, Zhao N, Jia P Y, Wang L and Li S Z 2020 *Appl. Phys. Lett.* **117** 134102

[29] Li X C, Chen J Y, Lin X T, Wu J C, Wu K Y and Jia P Y 2020 *Plasma Sources Sci. Technol.* **29** 065015

[30] Li X C, Geng J L, Jia P Y, Wu K Y, Jia B Y and Kang P C 2018 *Acta Phys. Sin.* **67** 075201 (in Chinese)

[31] Jia P Y, Gao K, Zhou S, Chen J Y, Wu J C, Wu K Y and Li X C 2021 *Plasma Sources Sci. Technol.* **30** 095021

[32] Wu K Y, Zhao N, Wu J C, Zhang F R, Niu M Y, Ran J X, Jia P Y and Li X C 2022 *Plasma Process. Polym.* **19** e2200003

[33] Wu K Y, Ren C H, Jia B Y, Lin X T, Zhao N, Jia P Y and Li X C 2019 *Plasma Process. Polym.* **16** e1900073

[34] Lu X, Laroussi M and Puech V 2012 *Plasma Sources Sci. Technol.* **21** 034005

[35] Ren C H, He X R, Jia P Y, Wu K Y and Li X C 2020 *Plasma Process. Polym.* **27** 113507

[36] Yu S, Chen Q Z, Liu J H, Wang K L, Jiang Z, Sun Z L, Zhang J and Fang J 2015 *Appl. Phys. Lett.* **106** 244101

[37] Lee J H, Kim Y H, Choi E H, Kim K M and Kim K N 2015 *Acta Odontol. Scand.* **73** 67

[38] Yoo E M, Uhm S H, Kwon J S, Choi H S, Choi E H, Kim K M and Kim K N 2015 *J. Biomed. Nanotechnol.* **11** 334

[39] Jeong W S, Kwon J S, Lee J H, Uhm S H, Choi E H and Kim K M 2017 *Biomed. Mater.* **12** 045015

[40] Yang Y, Guo J S, Zhou X, Liu Z Q, Wang C B, Wang K L, Zhang J and Wang Z M 2017 *Dent. Mater. J.* **37** 157

[41] Schoenbach K H, EI-Habachi A, Shi W and Ciocca M 1997 *Plasma Sources Sci. Technol.* **6** 468

[42] Stark R H and Schoenbach K H 1999 *Appl. Phys. Lett.* **74** 3770

[43] Moshkunov S I, Romanov K I, Khomich V Y and Shershunova E A 2021 *Plasma Phys. Rep.* **48** 449

[44] Wu J C, Wu K Y, Ren C H, Jia P Y and Li X C 2020 *Plasma Sci. Technol.* **22** 055505

[45] Li X C, Zhang P P, Bao W T, Jia P Y and Chu J D 2016 *Plasma Sources Sci. Technol.* **25** 025022

[46] Xian Y B, Wu S Q, Wang Z, Huang Q J, Lu X P and Kolb J F 2013 *Plasma Process. Polym.* **10** 372

[47] Xian Y B, Lu X P, Wu S Q, Chu P K and Pan Y 2012 *Appl. Phys. Lett.* **100** 123702

[48] Zhao N, Wu K Y, He X R, Chen J Y, Tan X, Wu J C, Ran J X, Jia P Y and Li X C 2022 *J. Phys. D: Appl. Phys.* **55** 015203

[49] Wu Y, Li Y H, Jia M, Liang H and Song H M 2012 *Chin. Phys. B* **21** 045202

[50] Mraihi A, Merbahi N, Yousfi M, Abahazem A and Eichwald O 2011 *Plasma Sources Sci. Technol.* **20** 065002

[51] Stancu G D, Kaddouri F, Lacoste D A and Laux C O 2010 *J. Phys. D: Appl. Phys.* **43** 124002

[52] Jia P Y, Chen M, Jia H X, Tan X, Ran J X, Wu K Y, Wu J C, Chen J Y, Pang X X, Li X C and Zhao N 2022 *IEEE Trans. Radiat. Plasma Med. Sci.* **7** 203

[53] Li X C, Zhou S, Gao K, Ran J X, Wu K Y and Jia P Y 2022 *IEEE Trans. Plasma Sci.* **50** 1717

[54] Paris P, Aints M, Valk F, Plank T, Haljaste A, Kozlov K V and Wagner H-E 2005 *J. Phys. D: Appl. Phys.* **38** 3894

[55] Yang L J, Song C H, Zhao N, Zhou S, Wu J C and Jia P Y 2021 *Acta Phys. Sin.* **70** 155201 (in Chinese)

[56] Li X C, Kang P C, Gao K, Zhou S, Wu K Y and Jia P Y 2020 *Plasma Process. Polym.* **17** e1900223

[57] Choi J H, Lee T I, Han I, Baik H K, Song K M, Lim Y S and Lee E S 2006 *Plasma Sources Sci. Technol.* **15** 416

[58] Li X C, Zhao N, Fang T Z, Liu Z H, Li L C and Dong L F 2008 *Plasma Sources Sci. Technol.* **17** 015017

[59] Chen J Y, Zhao N, Wu J C, Wu K Y, Zhang F R, Ran J X, Jia P Y, Pang X X and Li X C 2022 *Chin. Phys. B* **31** 065205

[60] Li X C, Jia P Y, Yuan N and Chang Y Y 2012 *Chin. Phys. B* **21** 045204

[61] Li X C, Yuan N, Jia P Y, Chang Y Y and Ji Y F 2011 *Acta Phys. Sin.* **60** 125204 (in Chinese)

[62] Zhu X M and Pu Y K 2010 *J. Phys. D: Appl. Phys.* **43** 403001

[63] Wang Y Y, Yan H J, Guo H F, Xu Y F, Zhang Q Z and Song J 2021 *Plasma Sources Sci. Technol.* **30** 075009

[64] Chen C J, Fang Z Q, Yang X F, Fan Y S, Zhou F and Wang R G 2022 *Chin. Phys. B* **31** 025204

[65] Cheng C, Shen J, Xiao D Z, Xie H B, Lan Y, Fang S D, Meng Y D and Chu P K 2014 *Chin. Phys. B* **23** 075204

[66] Liu Y F, Su C Q, Ren X, Fan C, Zhou W W, Wang F and Ding W D 2014 *Appl. Surf. Sci.* **313** 53

[67] Sun J, Yao L, Gao Z Q, Peng S J, Wang C X and Qiu Y P 2010 *Surf. Coat. Technol.* **204** 4101